Microlensing of Gamma#Ray Burst Afterglows

THE ASTROPHYSICAL JOURNAL, 495:597–603, 1998 March 10

MICROLENSING OF GAMMA-RAY BURST AFTERGLOWS

ABRAHAM LOEB AND ROSALBA PERNA
Harvard-Smithsonian Center for Astrophysics, 60 Garden Street, Cambridge, MA 02138
Received 1997 August 18; accepted 1997 October 17

ABSTRACT

The afterglow of a cosmological gamma-ray burst (GRB) should appear on the sky as a narrow emission ring of radius $\sim 3 \times 10^{16}$ cm $(t/\mathrm{day})^{5/8}$ that expands faster than light. After a day, the ring radius is comparable to the Einstein radius of a solar mass lens at a cosmological distance. Thus, microlensing by an intervening star can significantly modify the light curve and polarization signal from a GRB afterglow. We show that the achromatic amplification signal of the afterglow flux can be used to determine the impact parameter and expansion rate of the source in units of the Einstein radius of the lens, and we probe the superluminal nature of the expansion. If the synchrotron emission from the afterglow photosphere originates from a set of coherent magnetic field patches, microlensing would induce polarization variability as a result of the transient magnification of the patches behind the lens. The microlensing interpretation of the flux and polarization data can be confirmed by a parallax experiment that would probe the amplification peak at different times. The fraction of microlensed afterglows can be used to calibrate the density parameter of stellar-mass objects in the universe.

Subject heading: cosmology: theory — gamma rays: bursts — gravitational lensing

1. INTRODUCTION

The recent discovery of delayed X-ray (Costa et al. 1997), optical (van Paradijs et al. 1997; Bond 1997), and radio (Frail et al. 1997) emission over hours to several months following γ-ray bursts (GRB) established a new class of variable sources in astronomy. Of particular significance is the detection of Fe II and Mg II absorption lines at a redshift of $z = 0.835$ in the optical spectrum of GRB 970508 (Metzger et al. 1997), which confirmed the extragalactic origin of this burst. Since the source redshift must be higher than the absorber redshift, its required optical luminosity exceeds that of a supernova by several orders of magnitude. Thus, GRB afterglows might be detectable out to high redshifts. One could then use the signatures of absorption in the optical band (Metzger et al. 1997), scintillations in the radio regime (Goodman 1997), or gravitational lensing (Gould 1992; Mao 1993) by intervening material along the line of sight to study the intrinsic properties of afterglow sources.

Afterglows are most naturally explained by models in which bursts are produced by relativistically expanding fireballs (Paczyński & Rhoads 1993; Meszaros & Rees 1997; Vietri 1997a; Waxman 1997a, 1997b; Wijers, Rees, & Meszaros 1997; Vietri 1997b). On encountering an external medium, the relativistic shell that emitted the initial GRB decelerates and converts its bulk kinetic energy to synchrotron radiation, giving rise to the afterglow. The combined radio and optical data imply that the fireball energy is $\sim 10^{51-52}$ ergs. As a result of relativistic beaming, the emission region seen by an external observer occupies an angle of $\sim 1/\gamma$ relative to the center of the explosion, where γ is the Lorentz factor. This region appears to expand faster than the speed of light and occupies an angle of ~ 0.1–10^2 microarcseconds on the sky (or a physical size of $\sim 10^{15}$–10^{18} cm). Owing to the smallness of this angular size, it is difficult to resolve the afterglow source with terrestrial telescopes. However, the lensing zone of a solar mass lens located at cosmological distances occupies a microarcsecond on the sky (hence the term "microlensing"), and thus offers a unique opportunity for resolving GRB sources during their afterglow phase. Because of the superluminal expansion of the source, any (nonrelativistic) peculiar velocity of the lens relative to the source can be ignored. The amplification peak of a microlensing event lasts for only $\lesssim 1$ day, after which the net amplification weakens as the source size grows larger than the Einstein radius of the lens. The short duration of a microlensing event could therefore provide a test for the high Lorentz factor of the afterglow photosphere, which is predicted by all fireball models (for comparison, the variations due to peculiar velocities in microlensing events of steady sources take decades rather than days).

The rapid expansion and deceleration of the fireball causes a sharp decline in its surface brightness as a function of time. Since emission along the line of sight to the source center suffers from the shortest geometric time delay, it occurs at larger radii and appears dimmer than slightly off-axis emission. At any given time, the source is expected to appear as a narrow ring of radius R/γ and a width on the order of a tenth of this radius (Waxman 1997c). The outer cutoff is set by the sharp decline in relativistic beaming outside the ring. As the ring crosses a lens, its magnification adds a sharp peak to the otherwise smooth light curve of the afterglow. The sharpness of the peak depends on the thickness of the radiating gas layer behind the shock and on the shock deceleration rate. Microlensing could therefore provide important information about the structure and dynamics of the afterglow photosphere.

The probability for stellar microlensing of a source at a redshift $z_s \sim 1$ is $\sim 0.1\Omega_* b^2$ (Press & Gunn 1973; Gould 1995), where Ω_* is the mean density of stellar-mass objects in the universe in units of the critical density, and b is the impact parameter of the source relative to the lens in units of the Einstein radius. The known population of luminous stars amounts to $\Omega_* \sim 5 \times 10^{-3}$ (Woods & Loeb 1997), which implies that most cosmological sources are separated from stellar lenses by $b \sim 40$. The typical impact parameter is smaller by an order of magnitude if the dark matter is made of massive compact halo objects (MACHOs), as Galactic microlensing searches suggest (Alcock et al. 1997).

In this paper, we examine the question of whether a stellar-mass lens can resolve the predicted properties of afterglow photospheres. For concreteness, we derive numerical results for the fireball emission model of Waxman (1997b, 1997c). Since the afterglow occurs long after the explosive energy release, its properties are not sensitive to the spatial or temporal details of the point explosion that triggered the GRB. However, our adopted emission model is by no means a unique interpretation of the existing afterglow data (see, e.g., Vietri 1997a; Paczyński 1997); in fact, a future detection of a microlensing signal could serve to discriminate among competing afterglow models.

In § 2 we describe our model for GRB afterglows and characterize both the intensity and polarization signals that would result from a microlensing event. The numerical results and their implications are discussed in § 3. Finally, § 4 summarizes the main conclusions of this work.

2. SOURCE MODEL AND MICROLENSING SIGNATURES

2.1. *Source Model*

To illustrate the effects of microlensing on GRB afterglows, we need to specify the evolution of the source size and spectral intensity with time. We adopt the scaling laws for expansion and emission of a relativistic fireball that decelerates in a uniform ambient medium (Waxman 1997b).

In the fireball model, a compact ($\sim 10^6$–10^7 cm) source releases an energy of $E \sim 10^{52}$ ergs over $T \lesssim 10^2$ s with a negligible baryonic contamination ($\lesssim 10^{-5}\ M_\odot$). The high energy density at the source results in an optically thick pair plasma that expands and accelerates to relativistic velocities. After an initial acceleration phase, the thermal energy is converted to kinetic energy of the protons. A cold shell of thickness cT is formed and continues to expand. Internal shell collisions resulting from unsteady source activity could convert part of kinetic energy into radiation and yield the primary GRB emission via synchrotron emission and inverse Compton scattering (Paczyński & Xu 1994; Rees & Meszaros 1994; Sari, Narayan, & Piran 1996). As the cold shell expands, it impacts on the surrounding medium and drives a relativistic shock in it; this shock continuously heats fresh gas and accelerates relativistic electrons, which produce, via synchrotron emission, the delayed radiation observed on timescales of hours to months. Following Waxman (1997b), the radius of the shock at observed time t is given by

$$R(t) \approx 8.7 \times 10^{16} E_{52}^{1/4} n_1^{-1/4} t_{\rm hr}^{1/4}\ {\rm cm}\ , \tag{1}$$

while its Lorentz factor is

$$\gamma(t) = \sqrt{\frac{R(t)}{2ct}} \approx 21 E_{52}^{1/8} n_1^{-1/8} t_{\rm hr}^{-3/8}\ . \tag{2}$$

Here, E_{52} is the fireball energy in units of 10^{52} ergs, n_1 is the ambient gas density in cm^{-3}, and $t_{\rm hr}$ is the observed time in hours. As mentioned in § 1, most of the emission is seen from a narrow ring of radius

$$\rho_s(t) = \frac{R(t)}{\gamma(t)} \approx 4.1 \times 10^{15} E_{52}^{1/8} n_1^{-1/8} t_{\rm hr}^{5/8}\ {\rm cm}\ . \tag{3}$$

The width of the ring is a fraction $W \sim 10\%$ of its radius ρ_s if the thickness of the radiating layer behind the shock is determined by the shock hydrodynamics in a self-similar expansion (Waxman 1997c). A thicker radiating layer (e.g., due to a large gyroradius of the radiating electrons) would result in a wider ring. In § 3 we will show numerical results for different choices of W. These expressions are also valid for a jet geometry, as long as the opening angle of the jet is $\gtrsim 1/\gamma$.

The X-ray, optical, and radio emission following the γ-ray burst can be modeled as synchrotron emission from a power-law population of electrons within the heated shell behind the expanding shock. Under the assumption that the magnetic field energy density in the shell rest frame is a fraction ξ_B of the equipartition value, and that the power-law electrons carry a fraction ξ_e of the dissipated energy, the observed frequency at which the synchrotron spectral intensity of the electrons peaks is

$$\nu_m(t) = 2.4 \times 10^{16} \left(\frac{1+z_s}{2}\right)^{1/2} \left(\frac{\xi_e}{0.2}\right)^2 \left(\frac{\xi_B}{0.1}\right)^{1/2} E_{52}^{1/2} t_{\rm hr}^{-3/2}\ {\rm Hz}\ , \tag{4}$$

where z_s is the cosmological redshift of the source. For $\Omega = 1$ and $H_0 = 50$ km s^{-1} Mpc^{-1}, the observed intensity at ν_m is

$$F_{\nu_m} = 0.4 \left(\frac{1+z_s}{2}\right)^{-1} \left(\frac{1-1/\sqrt{2}}{1-1/\sqrt{1+z_s}}\right)^2 n_1^{1/2} \times \left(\frac{\xi_B}{0.1}\right)^{1/2} E_{52}\ {\rm mJy}\ . \tag{5}$$

If the distribution of electron Lorentz factors follows a power law, $dN_e/d\gamma_e \propto \gamma_e^{-p}$, with a low-energy cutoff set by ξ_e, then the observed intensity as a function of frequency, ν, obeys

$$F_\nu^0(t) = F_{\nu_m} \left[\frac{\nu}{\nu_m(t)}\right]^{-\alpha}\ , \tag{6}$$

where ν_m is the emission frequency of the electrons at the low-energy cutoff. The variation in ν_m across the finite width of the ring can be ignored for $W \ll 1$. The typical parameter values required to fit the afterglow data are $\xi_e \sim 0.2$, $\xi_B \sim 0.1$, and $p \sim 2$, so that $\alpha \sim 0.5$ for $\nu > \nu_m$ and $\alpha = -\frac{1}{3}$ for $\nu < \nu_m$.

2.2. *Flux Amplification Due to Microlensing*

We now consider a point lens of mass M and redshift z_l that happens to be located near the line of sight to an expanding fireball. We denote by η the impact parameter of the source center relative to the observer-lens axis.

For simplicity, we assume that the source has a uniform surface brightness in a ring of radius $\rho_s(t)$ (given by eq. [3]) and a width $W\rho_s(t)$. The flux seen by the observer is

$$F_\nu^{\rm lens}[t, R_s(t), W, b] = F_\nu^0(t) \mu[R_s(t), W, b]\ , \tag{7}$$

where $R_s \equiv \rho_s/r_{\rm E}$, and $r_{\rm E}$ is the Einstein radius of the lens projected on the source plane, $r_{\rm E} = [(4GM/c^2)(D_s D_{ls}/D_l)]^{1/2}$, with D_l, D_s, and D_{ls} being the angular diameter distance to the lens, to the source, and from the lens to the source, respectively. These distances all depend on the cosmological parameters. In this paper, we assume $\Omega = 1$, $\Lambda = 0$, and $H_0 = 50$ km s^{-1} Mpc^{-1}. The magnification factor for a normalized lens-source separation $b \equiv \eta/r_{\rm E}$ is

$$\mu(R_s, W, b) = \frac{\Psi(R_s, b) - (1-W)^2 \Psi[(1-W)R_s, b]}{1-(1-W)^2}\ , \tag{8}$$

where $\Psi(R_s, b)$ is the magnification for a uniform disk of radius R_s (Schneider, Ehlers, & Falco 1992),

$$\Psi(R_s, b) = \frac{2}{\pi R_s^2}\left[\int_{|b-R_s|}^{b+R_s} dr\,\frac{r^2+2}{\sqrt{r^2+4}}\arccos\frac{b^2+r^2-R_s^2}{2rb} + H(R_s-b)\,\frac{\pi}{2}\,(R_s-b)\sqrt{(R_s-b)^2+4}\right]. \quad (9)$$

Here $H(x)$ is the Heaviside step function. The integral in equation (9) can be expressed more explicitly as a sum of elliptic integrals (Witt & Mao 1994).

Other analytic results exist for more general surface brightness distributions (Heyrovský & Loeb 1997).

2.3. *Polarization Variability Due to Microlensing*

If the afterglow photosphere contains a finite set of discrete patches, each having a coherent magnetic field distribution, then the emergent synchrotron radiation will be polarized. For a power-law distribution of electron energies with an index p, the degree of linear polarization in each coherent patch is given by (Rybicki & Lightman 1979)

$$\Pi = \frac{p+1}{p+7/3}\,. \quad (10)$$

For the inferred value of $p \sim 2$ (Waxman 1997b), $\Pi \sim 0.7$. A microlens capable of resolving the source could then provide useful information about its magnetic field structure.

To illustrate the effect of microlensing on polarization, we adopt a toy model in which the emission ring is divided into a set of independent segments, each having a coherent distribution of magnetic field lines. The polarization in each segment is then modeled as a traceless, symmetric 2×2 tensor with a random orientation angle and a contraction of $(P_{\alpha\beta}P^{\alpha\beta})^{1/2} = \Pi$, given by equation (10). To simplify the computation, we subdivide the emission ring into N segments of equal area and nearly square shape. To each segment we assign a randomly oriented linear polarization. For the sake of concreteness, we assume that the number of segments and the orientation of their polarization stays constant during the lensing event. This assumption is reasonable, since the effect of lensing peaks during the short period of time when the ring crosses the lens (which is smaller than the expansion time by a factor of $W \ll 1$).

The net observed polarization is then given by

$$\langle \mathbf{P} \rangle = \frac{\sum_{i=1}^{N} \mathbf{P}_i A_i}{\sum_{i=1}^{N} A_i}\,, \quad (11)$$

where A_i and $\mathbf{P}_i$ are the area and polarization tensor of the ith segment, respectively, with

$$\mathbf{P}_i = \frac{\Pi}{\sqrt{2}}\begin{pmatrix}\cos 2\phi_i & \sin 2\phi_i \\ \sin 2\phi_i & -\cos 2\phi_i\end{pmatrix}, \quad (12)$$

and a random orientation angle, $0 \le \phi_i < 2\pi$.

We first consider the case in which there is no lensing, where $A_i = A_0 = \text{const}$ for $i = 1, \ldots N$. The two components of the net polarization are then given by

$$\langle P \rangle_{xx} = -\langle P \rangle_{yy} = \frac{\sum_{i=1}^{N} \Pi \cos 2\phi_i A_0}{\sqrt{2}NA_0} = \frac{\Pi}{\sqrt{2}N}\sum_{i=1}^{N}\cos 2\phi_i$$

$$\langle P \rangle_{xy} = \langle P \rangle_{yx} = \frac{\sum_{i=1}^{N} \Pi \sin 2\phi_i A_0}{\sqrt{2}NA_0} = \frac{\Pi}{\sqrt{2}N}\sum_{i=1}^{N}\sin 2\phi_i\,. \quad (13)$$

Clearly, the resulting polarization, $\langle P \rangle = [2(\langle P \rangle_{xx}^2 + \langle P \rangle_{xy}^2)]^{1/2}$, approaches zero for large N and is time independent.

Let us now consider the situation in which a lens is located at a projected position (x_l, y_l) with respect to the center of the source, so that $b = (x_l^2 + y_l^2)^{1/2}$. The observed polarization is still given by equation (11), but because of the stretching caused by lensing, the areas $\{A_i\}_{i=1}^{N}$ of the various segments are no longer equal,

$$A_i(t) = \int_i\int \zeta\, d\zeta\, d\theta\,\frac{d^2+2}{d\sqrt{d^2+4}}\,, \quad (14)$$

where (ζ, θ) are polar coordinates centered on the source, and the integrand is the point-source amplification factor at an impact parameter $d \equiv [(\zeta\cos\theta - x_l)^2 + (\zeta\sin\theta - y_l)^2]^{1/2}$. The integral is taken over the unlensed area of the segments. Because the size and position of the various segments relative to the lens change with time, the observed polarization will vary during a microlensing event.

3. NUMERICAL RESULTS

3.1. *Flux Amplification*

The solid lines in Figures 1 and 2 show the unlensed flux of an afterglow according to equation (6) and the parameter choices mentioned below that equation. The broken lines show the effect of microlensing on the observed flux, according to equation (7), for different choices of the ring's fractional width W, impact parameter b, and observed photon frequency ν.

The qualitative features of the microlensing signature on the afterglow light curve are as follows:

1. All wavelengths show the same amplification profile as a function of time.[1] While the amplification peak occurs on the rising side of the light curve in the radio, it appears on the declining side in X-rays, and might show on both sides of the break in the optical (see eq. [4] for the timing of the peak at a given frequency). The larger b is, the easier it becomes to detect the amplification signal at lower frequencies. For example, the optimal frequency for detecting a signal corresponding to $b = 1$ is $\sim 3 \times 10^{13}$ Hz (infrared wavelengths, ~ 10 μm), whereas it is an order of magnitude smaller for $b = 3$ (far-infrared wavelengths, ~ 100 μm). The achromaticity of the amplification peak can be used to separate the lensing signal from noise due to intrinsic variability or interstellar scintillations. Because scintillations only occur in the radio, a simple way to separate a lensing signature would be to cross-correlate the variability in the optical with that in the radio. Detailed observations of future afterglows are necessary in order to assess the characteristic level of intrinsic variability at different frequencies.

2. At early times, the temporal profiles of the lensed and unlensed fluxes have the same shape but different amplitudes. During this period, the source can still be regarded as pointlike, and the offset between the lensed and unlensed curves is set by the point source magnification factor at a constant b. The unknown value of b could therefore be inferred from this asymptotic offset in amplitude between the lensed and unlensed regimes.

[1] The variation of the relativistic Doppler effect across the ring might result in a slight chromaticity of the lensing signal, but we ignore it here.

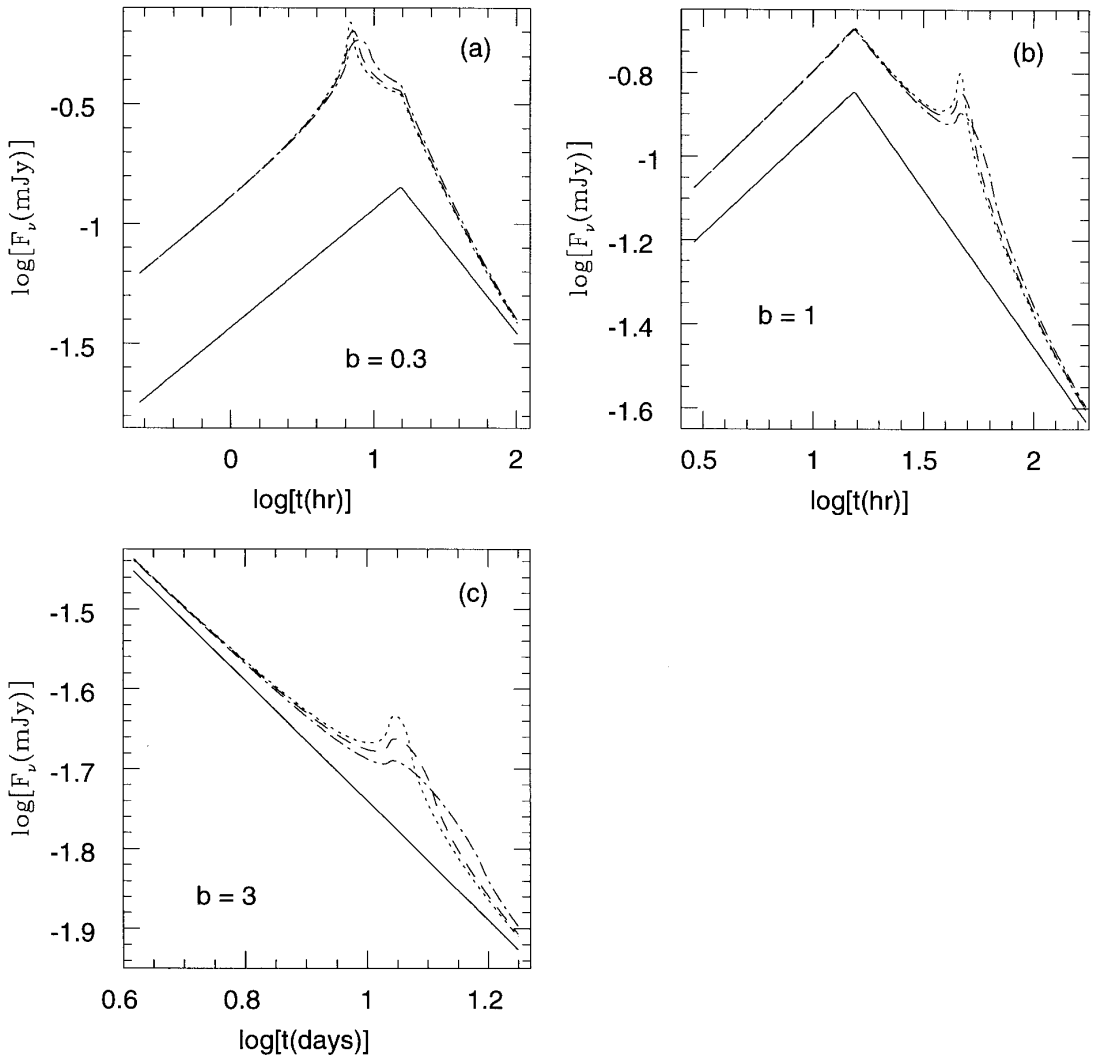

FIG. 1.—Unlensed (*solid line*) and lensed (*broken lines*) flux from a GRB afterglow with $E_{52} = 1$ and $n_1 = 1$ at a frequency of $\nu = 4 \times 10^{14}$ Hz. The different broken lines correspond to different fractional widths of the emission ring: $W = 5\%$ (*short-dashed line, highest peak*), 10% (*long-dashed line, middle peak*) and 20% (*dot-dashed line, lowest peak*). The lens mass is $M = 1\ M_\odot$, and its redshift is $z_l = 0.5$. The source redshift is $z_s = 2$. The likelihood for the events shown is $\sim(10\%–30\%)(\Omega_*/0.1)(b/3)^2$ (see Fig. 1 in Gould 1995).

3. The maximum amplification occurs at the time t_* when the ring crosses the lens, namely, when $R_s \sim b$. The otherwise unknown source size R_s can therefore be inferred at the time $t_*(b) \approx 2.3$ days $(br_E/5 \sim 10^{16}\ \mathrm{cm})^{8/5} E_{52}^{-1/5} n_1^{1/5}$, i.e., after several days for $b \sim 1$ and the characteristic Einstein radius of a solar mass lens at cosmological distances. By taking the ratio between the ring size and the period t_*, one finds the mean velocity of the expanding ring during that time interval in units of the Einstein radius, r_E. Given a probability distribution for r_E (based on a reasonable mass and redshift distribution for the lenses), one could then test the hypothesis of superluminal expansion.

4. Analysis of the shape of the light curve after the peak can provide more detailed information about the fractional width of the ring W and the temporal history of $R_s(t)$. The smaller W is, the higher and narrower the amplification peak gets. When $R_s \sim b$, the value of the magnification $\mu(R_s, W, b)$ becomes highly sensitive to the source size R_s. By monitoring the lensed flux as a function of time, one could infer the magnification $\mu_{obs}(t) = F_{obs}(t)/F_0(t)$, where $F_0(t)$ is found from the power-law extrapolation of the observed $F_{obs}(t)$ after the end of the microlensing event, to earlier times. Based on the magnification history $\mu_{obs}(t)$, one could infer the time evolution of $R_s(t)$ from the constraint $\mu(R_s, W, b) = \mu_{obs}(t)$, where $\mu(R_s, W, b)$ is given by equation (8) and b is inferred from point (2) above.

The quantitative interpretation of the lensing signatures suffers from an ambiguity about the physical size of the Einstein radius of the lens. This ambiguity can be removed through a parallax experiment, in which two (or more) telescopes, separated across the solar system, observe the same microlensing event with different values of b (Grieger, Kayser, & Refsdal 1986; Gould 1994). Since variability is induced by the superluminal expansion of the source (rather than by the motion of the lens, as is usually the case in microlensing events of steady sources), the two telescopes would simply observe different light curves with different values of b. Based on their known separation and their inferred b values (see point [2] above), one could then measure the physical size of the Einstein radius, r_E. The shape of the different peaks measured by the two telescopes

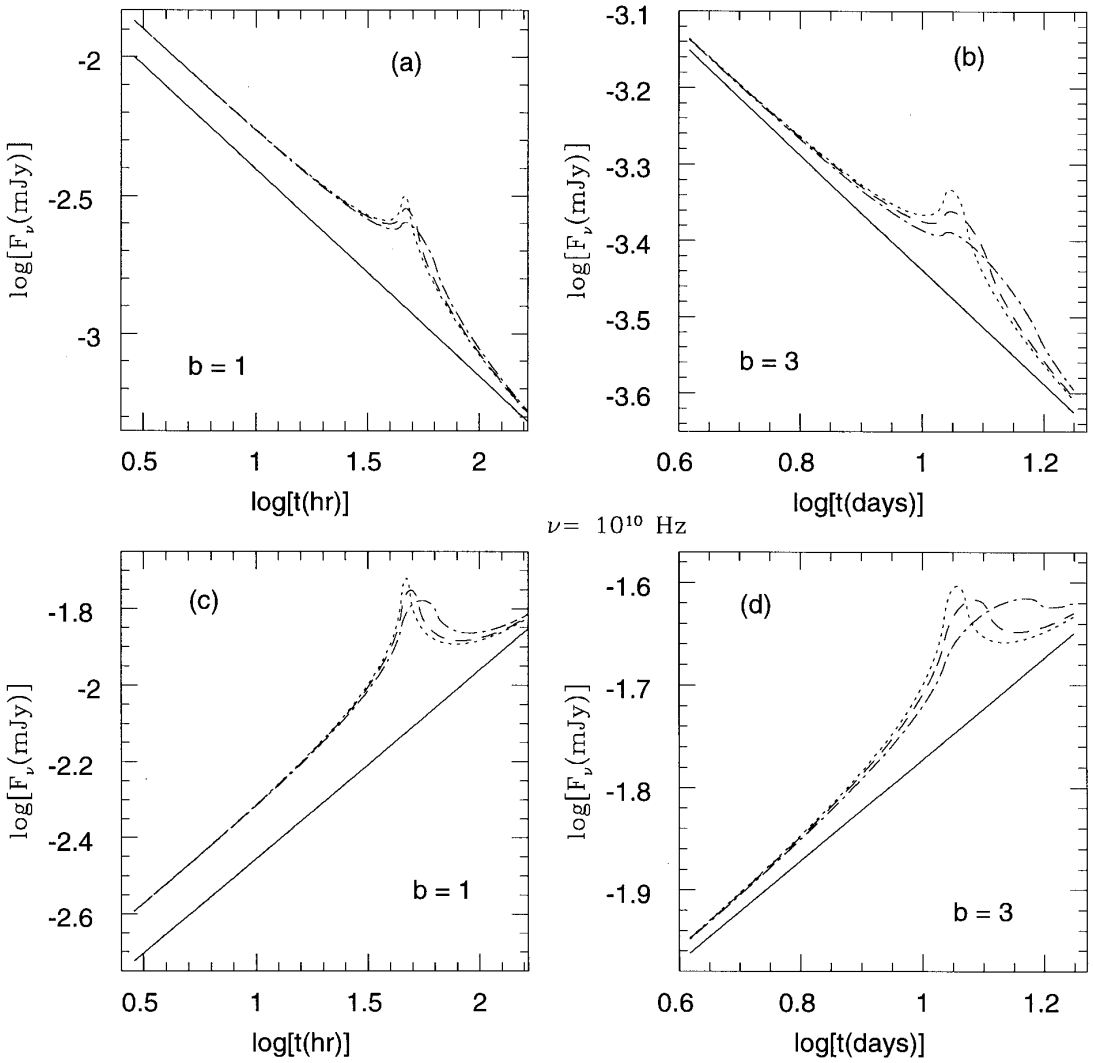

FIG. 2.—Same as in panels (*b*) and (*c*) of Fig. 1, but for different photon frequencies, i.e., in the X-ray (*panels a and b*) and radio (*panels c and d*) spectral regimes, for $\nu = 10^{18}$Hz.

can then be used to test for self-similarity in the shock structure and dynamics.

3.2. *Microlensed Polarization*

The different lines in Figure 3 show the deviation from the steady polarization signal predicted by equation (13) as a result of microlensing (eqs. [11] and [14]). The different panels show several random realizations for various choices of the lens-source separation b and the number of ring segments N. We consider two values of N, one in which the ring is composed of a single radial strip composed of nearly square segments ($N = 63$), and a second in which it is divided into two such strips ($N = 250$). The particular value that the polarization obtains at any given time t depends on the specific set of random orientation angles $\{\phi_i\}_{i=1}^{N}$ that were assigned to the segments in each realization, so the fluctuations induced by lensing should be analyzed on a statistical basis only.

The main qualitative characteristics of the lensing signal are:

1. The polarization changes around $t = t_*$ in coincidence with the flux amplification peak. At that time, the polarization fluctuates because as the ring expands, different segments approach the lens (and hence the point of maximum amplification) at different times. At any given time, the segment crossing the lens obtains the largest area in the image plane and provides the largest contribution to the overall polarization. The fluctuation rate increases as the area of each individual segment gets smaller (or as N gets larger), because smaller segments sweep faster across the lens.

2. If the ring is narrower than the Einstein diameter at lens crossing (i.e., $Wb \lesssim 1$), then the typical fluctuation amplitude, $\delta \equiv (\langle P \rangle / \langle P_0 \rangle) - 1$, is roughly independent of N (see Fig. 3, *top panels*). In this case, the ring is sliced into a fixed number of "effective" segments, each having a length on the order of the Einstein diameter, so that $N_{\rm eff} \sim (2\pi\rho_s)/(2r_{\rm E}) \sim \pi b$, and $\delta \sim N_{\rm eff}^{-1/2}$.

3. The fluctuation amplitude decreases with increasing b, because in this limit the highly magnified zone behind the lens amounts to a smaller fraction of the entire ring area.

4. CONCLUSIONS

We have shown that microlensing by stars can be used to study the size, superluminal expansion rate, and granularity of the photospheres of GRB afterglows. The light curves shown in Figures 1 and 2 can be used to extract the source

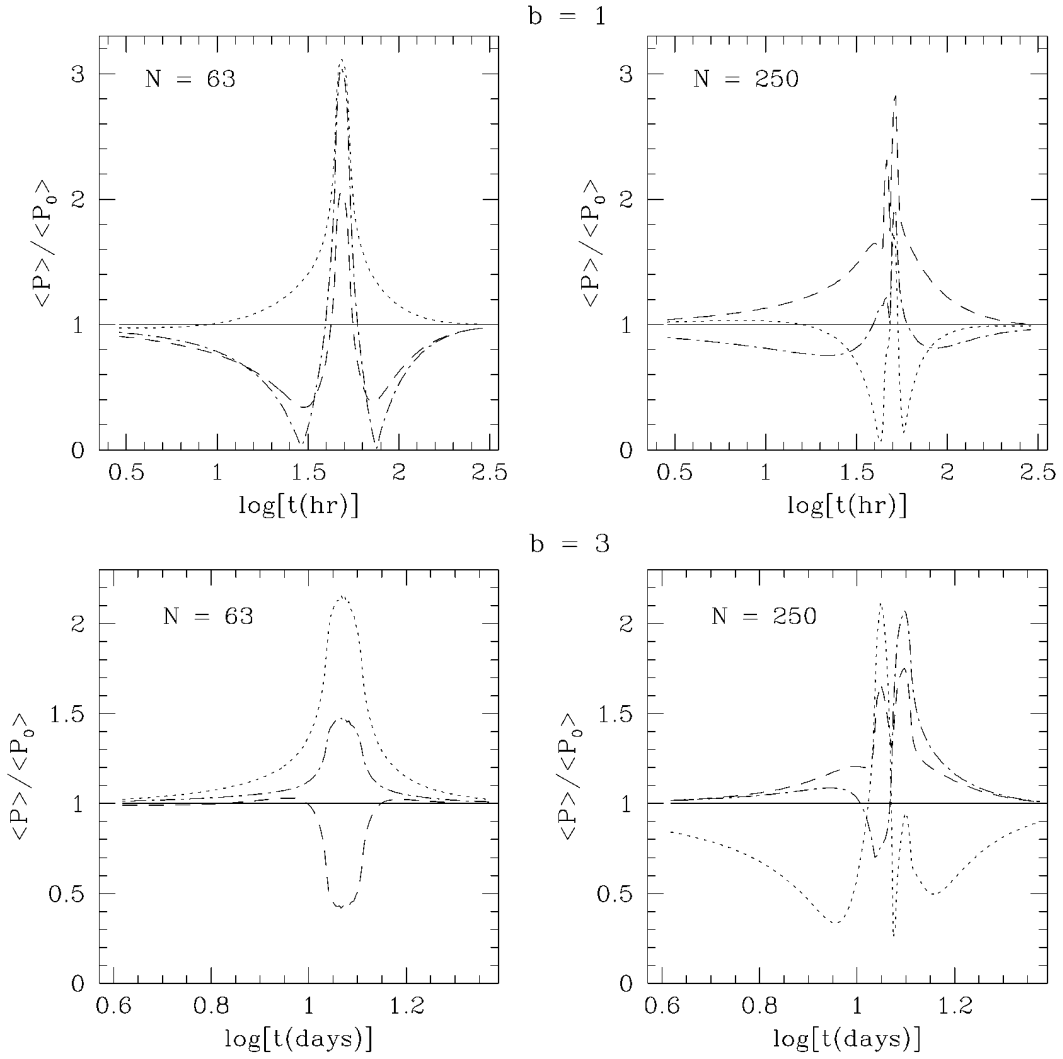

FIG. 3.—The lensed polarization signal, $\langle P \rangle$, normalized by the (constant) unlensed value $\langle P_0 \rangle$. The different lines show three random realizations of the time-varying polarization that would be observed during a microlensing event if the emission ring is composed of N nearly square segments that produce a polarization of equal amplitude but random orientation. Results are shown for different values of N and the source-lens separation b. The unlensed polarization is $\langle P_0 \rangle \approx 0.09$ and 0.04 for $N = 63$ and 250, respectively. Parameters are the same as in Fig. 1, with $W = 10\%$.

impact parameter b relative to the lens (based on the normalization offset between the pre- and postlensing curves), the fractional width of the emission ring (from the height and width of the amplification peak), and the source expansion rate and size in units of the Einstein radius of the lens. The source size can be measured explicitly through a parallax experiment that would obtain two (or more) light curves that sample the achromatic amplification peak at different times (cf. Figs. 1 and 2). Such an experiment could serve as the definitive tool for discriminating between a microlensing event and intrinsic variability of the afterglow source.

By monitoring the variability of the polarization with time during a microlensing event, it is also possible to estimate the number of coherent magnetic field patches on the afterglow photosphere (Fig. 3).

If the cosmological density parameter of stellar mass MACHOs is Ω_*, then most afterglow events will acquire an impact parameter $b \lesssim 10(\Omega_*/0.1)^{-1/2}$ from their nearest lens. Multiband photometry with an accuracy of ~ 0.03 mag could then detect the flux amplification signal shown in Figures 1 and 2 and test for its achromaticity, or else place interesting upper limits on Ω_* based on a relatively small sample of frequently monitored afterglows. The $\sim 10\%$ amplification signal shown in panel (c) of Figure 1 for $b = 3$ would appear in 1%–20% of all afterglows after a couple of weeks, at the time when the peak flux of $\sim$mJy is reached at far-infrared wavelengths, ~ 100 μm. A future X-ray satellite that could locate afterglows to within an arcminute (as does *BeppoSAX*) for all GRBs detected by BATSE might identify hundreds of afterglows per year, and could provide a rich sample for such microlensing studies.

Although our results were limited to isolated point lenses, their qualitative features should be common to lens systems with more complicated caustic structure, such as binary stars or galactic cores.

We thank Eli Waxman for valuable discussions and for communicating results from his work prior to publication, and David Heyrovský for useful comments on the manuscript. This work was supported in part by the NASA ATP grant NAG5-3085 and the Harvard Milton fund.

REFERENCES

Alcock, C., et al. 1997, ApJ, 479, 119
Bond, H. E. 1997, IAU Circ. 6654
Costa, E., et al. 1997, Nature, 387, 783
Frail, D. A., et al. 1997, ApJ, 483, L91
Goodman, J. 1997, preprint astro-ph/9706084
Gould, A. 1992, ApJ, 386, L5
———. 1994, ApJ, 421, L75
———. 1995, ApJ, 455, 37
Grieger, B., Kaiser, R., & Refsdal, S. 1986, Nature, 324, 126
Heyrovský, D., & Loeb, A. 1997, ApJ, 490, 38
Mao, S. 1993, ApJ, 402, 382
Meszaros, P., & Rees, M. J. 1997, ApJ, 476, 232
Metzger, M. R., et al. 1997, IAU Circ. 6655
Paczyński, B. 1997, ApJL, submitted (preprint astro-ph/9706232)
Paczyński, B., & Rhoads, J. E. 1993, ApJ, 418, L5
Paczyński, B., & Xu, G. 1994, ApJ, 427, 708
Press, W. H., & Gunn, J. E. 1973, ApJ, 185, 397
Rees, M. J., & Meszaros, P. 1994, ApJ, 430, L93
Rybicki, G. B., & Lightman, A. P. 1979, Radiative Processes in Astrophysics (New York: Wiley)
Sari, R., Narayan, R., & Piran, T. 1996, ApJ, 473, 204
Schneider, P., Ehlers, J., & Falco, E. E. 1992, Gravitational Lenses (Berlin: Springer), 313
van Paradijs, J., et al. 1997, Nature, 386, 686
Vietri, M. 1997a, ApJ, 478, L9
———. 1997b, ApJ, 488, L105
Waxman, E. 1997a, ApJ, 485, L5
———. 1997b, ApJ, 489, L33
———. 1997c, ApJ, 491, L19
Wijers, A. M., Rees, M. J., & Meszaros, P. 1997, MNRAS, 288, L51
Witt, H. J., & Mao, S. 1994, ApJ, 430, 505
Woods, E., & Loeb, A. 1997, ApJ, 453, 583